Dynamic Performances of Split-shaft Microturbine Generator (MTG) System In Stand-alone Mode and When Connected to a Rural Distribution Network

Bikash Das and Debapriya Das

ABSTRACT

The article presents the dynamic analysis of split-shaft microturbine coupled with synchronous generator. Dynamic studies of microturbine generator (MTG) system are investigated considering both speed controller and load following controller. It is shown that speed controller is necessary for MTG system when there is a sudden increase or decrease of load demand with respect to the reference set point. A new load following controller with a frequency deviation as an input signal to it, is also proposed and eliminates the need of a speed controller for MTG system for variations of load demand. Finally MTG system is connected to an 11 kV rural distribution network to examine the transient behavior during active power injection. Simulation results for various cases are presented.

Keywords: Split-shaft microturbine, synchronous generator, load following controller, speed controller, rural distribution network.

INTRODUCTION

Due to restructuring of electric utility and increase of power demand, distribution energy resources (DERs) have received significant attention for improving the performance and reliability of power system. Application of DERs also reduces the transmission and distribution power losses and improves the power quality. Distributed energy resources may include fuel cells, photovoltaic cells, minihydro, wind turbine generators and microturbine generators (MTGs) etc. Also from the public environmental policy, lots of scope is there for large-scale in-

tegration of DERs into distribution system [1]. MTGs are quite useful for peak saving customer's base-load requirements, or can be used for stand by and cogeneration applications.

Microturbines are small and simple-cycle gas turbine with output ranging from 25 kW to 500 kW. There are essentially two types of microturbines. One is high speed single-shaft unit with the compressor and turbine mounted on the same shaft as the electrical alternators; turbine speeds mainly range from 50,000 rpm to 120,000 rpm. The high frequency ac voltage generated by the alternator is converted to standard power frequency voltage through the power electronic interfaces. The other type of microturbine is a split-shaft design that uses as power turbine rotating at 3000 rpm/3600 rpm and a conventional induction machine or synchronous machine connected via a gearbox for speed multiplications. Development of microturbines technology is reported in several references [2, 3, 4].

Several researchers have studied the dynamic analysis of a MTG system. Zhu and Tomsovic [5] have studied the load following performance of MTG and fuel cells. Their analysis reveals that the MTG system is capable of providing load following service. El-Sharkh et al [6] have also studied the load following behavior of MTG and fuel cells. Their model includes a speed controller to bring back the frequency to its nominal value. Saha et al [7] have also studied the load following behavior of a MTG system for different loading conditions. Wang and Zheng [8] have also studied the power-electronics based MTG system connected to distribution network. Jurado and Saenz [9] have proposed an adaptive control technique for hybrid power system with fuel cells and MTG system. Ho et al [10] have studied the dynamic performance of a MTG system for cogeneration application. Bertani et al [11] have also studied the dynamic behavior of MTG system for both islanding and grid connected modes.

Most of the single-shaft MTG systems use a permanent magnet synchronous generator (PMSG) or asynchronous generator for generation of power, and the operation of MTG system is considered in islanding or grid connected mode [1, 11, 12]. Single-shaft configuration with asynchronous generator or PMSG is simple and power electronics rectifier-inverter is used to supply power to the load at nominal voltage and frequency [5, 11, 12]. Single-shaft high speed PMSG has some drawbacks such as high centrifugal forces, more thermal stress, rotor losses due to fringing effects, demagnetization effect, high cost etc. [11, 12]. On

the other hand, induction generators are cost effective and robust but their speed depends on load and require grid interface through power electronics converter systems.

Very few researchers [7, 13] have studied the dynamic analysis of microturbines with a synchronous generator (SG) but complete block diagram representation of such MTG system equipped with speed controller and load following controller is not available in the literature [7, 13].Main advantage of split-shaft configuration is that it does not require an inverter to convert the frequency of the ac power. Another advantage of coupling a split-shaft microturbine with synchronous generator is that it eliminates the use of rectifier and power converter. In this case, the turbine is connected to generator via a gearbox to generate standard 50/60 Hz power.

In this article, a split-shaft Microturbine coupled with an SG is used to study the load following performance in stand-alone mode and also its performance when it is connected to a rural distribution network. Main focus of this article is active power control. A proportional-integral (P-I) type speed controller is used along with a P-I type of load following controller.

It is also shown that a load following controller can also act as a speed controller, if frequency deviation is used as an input signal to the load following controller and hence eliminates the need of a speed controller. To the best of the authors knowledge, this important issue was not addressed by the previous researchers for MTG system. Another aspect of this research work is the performance of MTG system when it is connected to a rural distribution network and this issue was also not addressed by the previous researchers for MTG system.

MODELING OF SPLIT-SHAFT MTG SYSTEM

Zhu and Tomsovic [1] have presented the details modeling of split-shaft microturbine system. They have modeled this split-shaft microturbine as a simple-cycle, single-shaft gas turbine. The GAST model is most commonly used dynamic model of gas turbine units without droop. It is a Western System Coordinating Council (WSCC) compliant model and the model is simple and follows typical modeling guideline [14]. Microturbine does not use any governor and hence governor model is omitted. In this work, the authors have used the widely accepted GAST turbine

model. The main blocks of MTG system are shown in Figure 1. In Figure 1, damping of turbine is neglected as its effect on dynamic performances is negligible [5, 7, 14].

The microturbine output being the mechanical power change ΔP_m. If ΔP_{Le} represents an electrical load change, the difference (ΔP_m - ΔP_{Le}) is absorbed by the power system, where the MTG system is connected. Now (ΔP_m - ΔP_{Le}) is accounted for in two ways [15, 16]:

I. Rate of increase of stored kinetic energy (KE) in the generator rotor. At scheduled system frequency (f_0), the stored energy is

$$W_{ke}{}^0 = H \times P_r \text{ kW-Sec} \tag{1}$$

Where

P_r = rated capacity of MTG (kW)
H = inertia constant (Sec).

The kinetic energy is proportional to square of the speed (hence frequency). The kinetic energy at frequency ($f_0 + \Delta f$) is given by

$$W_{ke} = W_{ke}{}^0 \left(\frac{(f_0 + \Delta f)}{f_0} \right)^2$$

$$\therefore \quad W_{ke} \approx HP_r \left(1 + \frac{2\Delta f}{f_0} \right)$$

$$\therefore \quad \frac{d}{dt}(W_{ke}) = \frac{2HP_r}{f_0} \frac{d}{dt}(\Delta f) \tag{2}$$

II. It is assumed that the load is sensitive to the speed (frequency) variation. However, for small change in system frequency Δf, the rate of change of load with respect to frequency, that is $\frac{\partial P_{Le}}{\partial f}$ can be regarded as constant. This load changes can be expressed as:

10% Online Discount Use Code JR10

RESIDENTIAL ENERGY AUDITING AND IMPROVEMENT

Stan Harbuck and Donna Harbuck

Here is your complete guide to the effective practice of residential energy auditing, covering in detail the specific procedures, techniques and standards practiced within the profession today. The book is intended for use as an educational resource by energy auditors or residential retrofitters, whether working in a weatherization program or in the private arena. Specific topics include the house as a system, the auditor's tools, weatherization, sealants, insulation and barriers, retrofitting, heating and cooling, base load, and new construction. The content of this book is also designed to serve as a preparatory vehicle for auditors seeking to achieve several professional certifications, including programs offered by BPI, RESNET-HERS, DOE/NREL and AEE. Appendices provide a wealth of valuable information, covering weatherization standards and calculations, math basics, conversion tables, climate data, insulation assessments, utility bill interpretation and more.

ISBN: 0-88173-726-7

6 x 9, 660 pp., Illus.
Hardcover

$150
Order Code 0694

CONTENTS

BOOK ORDER FORM

① Complete quantity and amount due for each book you wish to order:

Quantity	Book Title	Order Code	Price	Amount Due
	Residential Energy Auditing and Improvement	**0694**	**$150.00**	

② Indicate shipping address: CODE: Journal 2014

NAME (Please print) BUSINESS PHONE

SIGNATURE (Required to process order) EMAIL ADDRESS

COMPANY

STREET ADDRESS ONLY (No P.O. Box)

CITY, STATE, ZIP

Applicable Discount	
Georgia Residents add 6% Sales Tax	
Shipping $10 first book $4 each additional book	**10.00**
TOTAL	

MEMBER DISCOUNTS—A 15% discount is allowed to AEE members (discounts cannot be combined).

☐ **AEE Member (Member No._____)**

③ Select method of payment:

☐ **CHECK ENCLOSED**

Make check payable in U.S. funds to: **AEE ENERGY BOOKS**

☐ **CHARGE TO MY CREDIT CARD**

☐ *VISA* ☐ *MASTERCARD* ☐ *AMERICAN EXPRESS*

CARD NO.

Expiration date *Signature*

④ Send your order to:
AEE BOOKS
P.O. Box 1026
Lilburn, GA 30048

INTERNET ORDERING
www.aeecenter.org/books
(use discount code)

TO ORDER BY PHONE
Use your credit card and call:
(770) 925-9558

TO ORDER BY FAX
Complete and Fax to:
(770) 381-9865

INTERNATIONAL ORDERS
Must be prepaid in U.S. dollars and must include an additional charge of $10.00 per book plus 15% for shipping and handling by surface mail.

10% Online Discount Use Code JR10

BOILER OPERATOR'S HANDBOOK, 2nd Edition

Distributed Generation and
Kenneth E. Heselton, P.E.

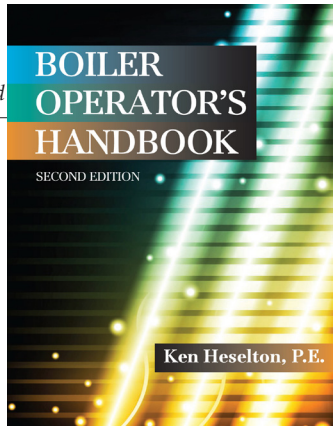

This book was written specifically for boiler plant operators and supervisors who want to learn how to lower plant operating costs, as well as how to operate plants of all types and sizes more wisely. This newly revised edition provides guidelines for HRSGs, combined cycle systems, and environmental effects of boiler operation. Also included is a new chapter on refrigeration systems which addresses the environmental effects of inadvertent and intentional discharges of refrigerants. Going beyond the basics of "keeping the pressure up," the author explains in clear terms how to set effective priorities to assure optimum plant operation, including safety, continuity of operation, damage prevention, managing environmental impact, training replacement plant operators, logging and preserving historical data, and operating the plant economically.

ISBN: 0-88173-730-5

8½ x 11, 488 pp., Illus.
Hardcover

$175
Order Code 0696

CONTENTS

BOOK ORDER FORM

① Complete quantity and amount due for each book you wish to order:

Quantity	Book Title	Order Code	Price	Amount Due
	Boiler Operator's Handbook, 2nd Edition	**0696**	**$175.00**	

② Indicate shipping address: CODE: Journal 2014

NAME (Please print) BUSINESS PHONE

SIGNATURE (Required to process order) EMAIL ADDRESS

COMPANY

STREET ADDRESS ONLY (No P.O. Box)

CITY, STATE, ZIP

Applicable Discount	
Georgia Residents add 6% Sales Tax	
Shipping $10 first book $4 each additional book	**10.00**
TOTAL	

MEMBER DISCOUNTS—A 15% discount is allowed to AEE members (discounts cannot be combined).

☐ **AEE Member (Member No._____)**

③ Select method of payment:

☐ **CHECK ENCLOSED**

☐ **CHARGE TO MY CREDIT CARD**

☐ *VISA* ☐ *MASTERCARD* ☐ *AMERICAN EXPRESS*

CARD NO.

Expiration date *Signature*

Make check payable in U.S. funds to:
AEE ENERGY BOOKS

④ Send your order to:
AEE BOOKS
P.O. Box 1026
Lilburn, GA 30048

INTERNET ORDERING
www.aeecenter.org/books
(use discount code)

TO ORDER BY PHONE
Use your credit card and call:
(770) 925-9558

TO ORDER BY FAX
Complete and Fax to:
(770) 381-9865

INTERNATIONAL ORDERS
Must be prepaid in U.S. dollars and must include an additional charge of $10.00 per book plus 15% for shipping and handling by surface mail.

$$\left(\frac{\partial P_{Le}}{\partial f}\right).\Delta f = D'.\Delta f$$

$$\text{Where} \quad D' = \frac{\partial P_{Le}}{\partial f} = \text{constant.} \tag{3}$$

Therefore, the power balance equation can be written as:

Hence,

$$\Delta P_m(pu) - \Delta P_{Le}(pu) = \frac{2H}{f_0}\frac{d}{dt}(\Delta f) + D\Delta f \tag{4}$$

Where $D = \frac{D'}{P_r}$ (5)

In Eqn. (4), ΔP_m and ΔP_{Le} are now in per unit (pu) values.
Taking the Laplace transform of Eqn. (4), we get:

$$\Delta f(s) = \frac{\Delta P_m(s) - \Delta P_{Le}(s)}{\left(D + \frac{2H}{f_0}s\right)}$$

$$\therefore \quad \Delta f(s) = \left[\Delta P_m(s) - \Delta P_{Le}(s)\right] \times \frac{K_p}{1 + sT_p} \tag{6}$$

$$T_p = \frac{2H}{Df_0} = \text{power system time constant.}$$

$$K_p = \frac{1}{D} = \text{gain of power system.}$$

Where,

$$T_p = \frac{2H}{Df_0} = \text{power system time constant.}$$

$$K_p = \frac{1}{D} = \text{gain of power system.}$$

In Figure 1, power system block is also shown. Other blocks in Figure 1, are Low Value Gate (LVG), Burner, Turbine and Temperature control loop are well defined in [5, 6, 12]. In addition to that, speed controller and load following controller are also shown in Figure 1. The main focus of this article is on the electric-mechanical behavior of the system at normal operating conditions. Fast dynamics such as loss of power, faults, start up and shutdown transients are not considered in this study.

DYNAMIC ANALYSIS OF THE MTG SYSTEM

Dynamic performances of the MTG system shown in Figure 1, are carried out for different cases. For all the cases, it was assumed that initially MTG system was running on no-load for 10 sec. Gain parameters of the speed controller and load following controller are selected by trial and error and for all the case studies, these gain parameters are kept fixed. Parameters of the system are given in Appendix.

Case-1: In this case, load demand P_{Le} = 0.4 pu and P_{ref} was set to 0.4 pu. Only load following controller is in operation and no speed controller is used ($K''_p = 0$, k''_i). Figure 2 shows the dynamic response of power output and Figure 3 shows the dynamic response of frequency deviation. From Figure 2 it is seen that the microturbine power output takes about 40 sec to match the load. From Figure 3 it is seen that the frequency deviation (Δf) at steady state is zero, although there was no speed controller. This is obvious, because P_{ref} = 0.4 pu and load demand P_{Le} = 0.4 pu and microturbine output power exactly chasing the load demand.

Case-2: In this case load demand has increased from 0.4 pu to 0.5 pu, i.e. P_{Le} = 0.5 pu and P_{ref} = 0.4 pu. Load following controller is in operation and no speed controller is used ($K''_p = 0$, $K''_i = 0$). Figure

4 shows the response of microturbine power output and Figure 5 shows the response of frequency deviation (Δf). From Figure 4 it is seen that the microturbine power output at steady state is 0.4 pu because P_{ref} = 0.4 pu. As the load demand P_{Le} (= 0.5 pu) is greater than the set value P_{ref} (= 0.4 pu) and no speed controller is used, at steady state there is an error in frequency deviation (Figure 5).

Case-3: In this case, condition is same as given in Case-2 but load following controller and speed controller are both in operation. Figure 6 shows the response of output power and Figure 7 shows the response of frequency deviation. From Figure 6 it is seen that at steady state, microturbine output power is equal to the load demand P_{Le} = 0.4 pu. This has happened because speed controller was in operation to make the frequency deviation zero at steady state (Figure 7).

From the above studies (Case-1, Case-2 & Case-3) it is clear that when $P_{ref} = P_{Le}$, no speed controller is required. However, if $P_{ref} \neq P_{Le}$, there will be a steady state error in frequency deviation and in this case operation of speed controller is must to make the frequency deviation zero at steady state.

USE OF FREQUENCY DEVIATION AS AN INPUT SIGNAL TO THE LOAD FOLLOWING CONTROLLER

In this section, it will be shown that if we use frequency deviation (Δf) through a proportional gain □ as an input signal to the load following controller, then no speed controller is required for MTG system. Structure of MTG system with such controller is shown in Figure 8.

Case-4: In this case P_{ref} is set to 0.4 pu and load demand P_{Le} = 0.4 pu (i.e. condition is same with Case-1) and the load following controller with a frequency deviation signal as an input to it as shown in Figure 8 is used. Figure 9 shows the power output response and Figure 10 shows the frequency deviation (Δf) response. For the purpose of comparison, dynamic responses as obtained in Case-1 is also shown in Figures 9 &10 respectively. From these figures, it is seen that power output is exactly matching the load demand and frequency deviation is zero at steady state. Comparing the dynamic

responses of Case-4 and Case-1, from Figures 9 and 10, it is found that when frequency deviation is applied to the load following controller as an input, peak deviation and settling time are less as compared to that obtained with Case-1.

Case-5: In this case P_{ref} = 0.4 pu but the load demand has increased from 0.4 pu to 0.5 pu, i.e. P_{Le} = 0.5 pu (condition is same with Case-2). Load following controller as shown in Figure 8 is used. Figure 11 shows the dynamic response of power output. From Figure 11 it is seen that, although P_{ref} = 0.4 pu, but microturbine power output is exactly matching the load demand P_{Le} = 0.5 pu because in this case frequency deviation is used as an input signal to the load following controller (Figure 8). Figure 12 shows the dynamic response of frequency deviation and it is seen that at steady state frequency deviation settles to zero. The dynamic responses of this case (Case-5) is compared with the dynamic responses of Case-2, which can be seen in Figures 11 and 12 respectively. It can be noticed in Figure 12 that when only load following controller was used there was an error in frequency deviation and power generation was not matching with the load demand at steady state, but when frequency deviation is applied as an input to the load following controller the frequency deviation become zero at steady state and the at steady state the power generation is same with the load demand.

Case-6: In this case P_{ref} = 0.4 pu but the load demand has decreased from 0.4 pu to 0.3 pu. Same load following controller as shown in Figure 8 is used. Figure 13 shows the dynamic response of power output and it is also seen that the power output settles to the value of load demand P_{Le} = 0.3 pu at steady state. Figure 14 shows the dynamic response of frequency deviation and at steady state frequency deviation settles to zero.

From the above analysis (Case-4, Case-5 & Case-6), it may be concluded that the speed controller of MTG system is not required if frequency deviation is given as an input signal to the load following controller. Another advantage of such MTG control scheme as shown in Figure 8 is that, if there is any change in load demand, there is no need to change the power reference set point of load following controller by the MTG operator and the output of MTG system will automatically follow the load demand.

EFFECT OF ACTIVE POWER PENETRATION IN A RURAL RADIAL DISTRIBUTION NETWORK

Figure 15 shows a 12 node 11 kV rural radial distribution network. MTG system is connected at node8througha 440 V/11kV (Δ - □) transformer. Data for this distribution system is given in Appendix. For MTG system, P_{ref} = 0.6 (150 kW) was set. Figures 16, 17, 18 and 19 show the dynamic responses during transient imbalance. From Figure 16 it is seen that power output of MTG system settles to 0.6 pu at steady state. From Figure 17 it is seen that frequency deviation settles to zero at steady state. Figure 18 shows the dynamic response of voltage magnitude of node 12during transient imbalance and at steady state voltage profile has improved due to active power penetration by MTG system. Similarly, Figure 19 shows the active power loss variation during transient imbalance and at steady state active power loss has decreased.

Before connecting MTG system to distribution system, total active power loss was 20.71 kW and after connecting MTG system to distribution network, total loss is 12.01 kW. Table–1 gives the steady state voltage magnitude of the network before and after connecting MTG system to the distribution network. There has been significant improvement of voltage profile after the connection of MTG system to the radial distribution network.

CONCLUSIONS

In this work, dynamic analysis of MTG system has been studied considering P-I type speed controller and P-I type load following controller. Analysis reveals that when reference power set point is equal to load demand, then load following controller forces the MTG power output to match the load demand at steady state and hence frequency deviation settles to zero at steady state and no speed controller is required. However, if load demand and reference power set point are not equal then operation of both speed controller and load following controller are required.

A new P-I type load following controller with frequency deviation as an input signal to it has also been proposed for MTG system. Advantage of such MTG control scheme is that it automatically follows the variations of load demand and no need to change the power reference

set point of load following controller by the MTG operator and also eliminates the need of a speed controller and gives better dynamic responses in terms of peak deviation and settling time.

Dynamic responses of MTG system has also been examined when it is connected to a rural distribution network. It was found that during transient imbalance, its performance was satisfactory and at steady state it improves the voltage profile and reduces the power loss of the network by 42%.

References

[1] Zhu Y, Tomsovic K. Optimal power flow for systems with distributed energy resources. Int J of Electrical Power Energy Syst 2007; 29(3): 260-7.
[2] Suter M. Active filter for a microturbine. In: Proc Inst Electrical engineering, Telcom energy conference (INTELEC2001), Edinburgh, UK; 2001. p. 162-5.
[3] Nichols D K, Loving K P. Assessment of microturbine generators. In: Proc IEEE PESGM, Vol.4; 2003. p. 2314-5.
[4] Peirs J, Reynaerts D, Verplaetsen F. A microturbine for electric power generation. Sensor Actuators 2004; 113(1): 86-93.
[5] Zhu Y, Tomsovic K. Development of models for analyzing the load-following performance of Microturbines and fuel cells. Electric Power System Research 2002; 62(1): 1-11.
[6] El-Sharkh M Y, Sisworahardjo N S, Uzunoglu M, Onar O, Alam M S. Dynamic behavior of PEM fuel cell and Microturbine power plants. Journal of Power Sources 2007;164(1): 315-21.
[7] Saha A K, Chowdhury S, Chowdhury S P, Crossley P A. Modeling and performance analysis of a microturbine as a distributed energy resource. IEEE Trans on Energy Conversion 2009; 24(2):529-38.
[8] Wang L, Zheng Guang-Zhe. Analysis of a microturbine generator system connected to a distribution system through power-electronics converters. IEEE Trans on Sustainable Energy 2011; vol.2, No.2, 159-66.
[9] Jurado F, Saenz J R. Adaptive control of a fuel cell – microturbine hybrid power Plant. IEEE Trans on Energy Conversion 2003; 18(2): 342-7.
[10] m for cogeneration application. Renewable Energy 2004; 29(7): 1121-33.
[11] Bettani A, Bossi C, Fornari F, Massucco S, Spelta S, Tivegna F. A microturbine generation system for grid connected and islanding operation. In: Proc IEEE Power System Conference, Expo (PES), vol.1; 2004. p. 360-5.
[12] Al-Hinai A, Feliachi A. Dynamic model of a microturbine used as a distributed generator. In: Proc IEEE System Theory, 2002. p. 209-13.
[13] Kalantar M, Mousavi G S M. Dynamic behavior of a Stand-alone hybrid power generation system of wind turbine, microturbine, solar array and battery storage. Applied Energy 2010; 87(10): 3051-64.
[14] Nagpal M, Moshref A, Morison G K. Experience with testing and modeling of gas turbines. In: Proc IEEE/PES, Winter Meeting, Columbus, Ohio, USA, vol.2, 2001. p. 652-6.
[15] Elgerd O.I. Electric energy systems theory an introduction. New Delhi: Tata-McGraw-Hill; 1983.
[16] Das D. Electrical power systems. New Age International (P) Limited Publication; 2006.

APPENDIX: Figures and Tables

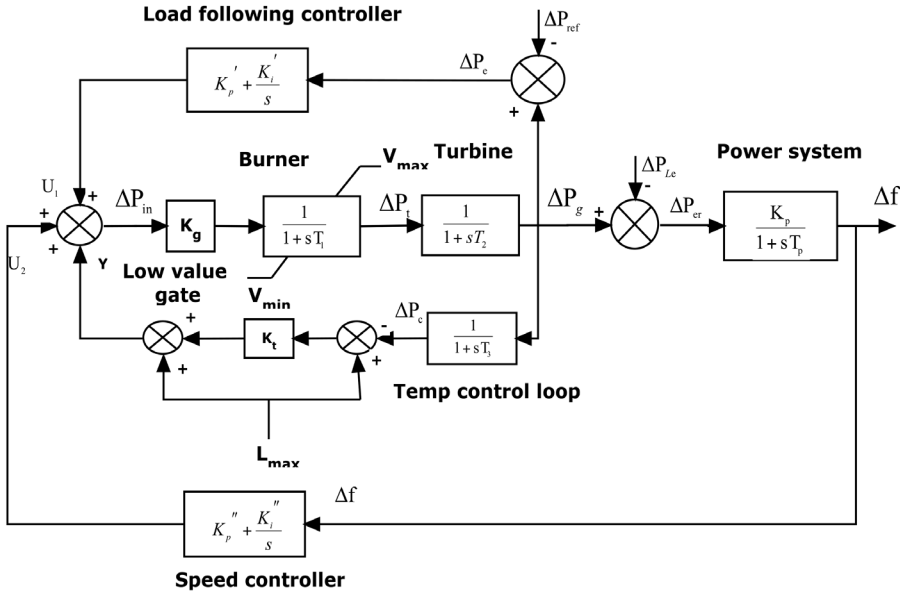

Figure 1: Block diagram representation of split-shaft MTG system equipped with P-I type speed controller and P-I type load following controller.

Case 1:

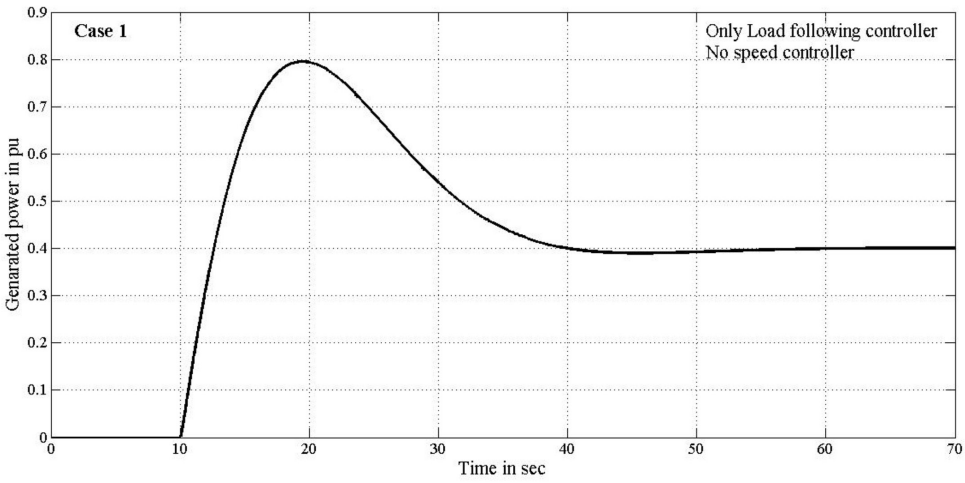

Figure 2: Generated power by MTG system in pu (Case-1)

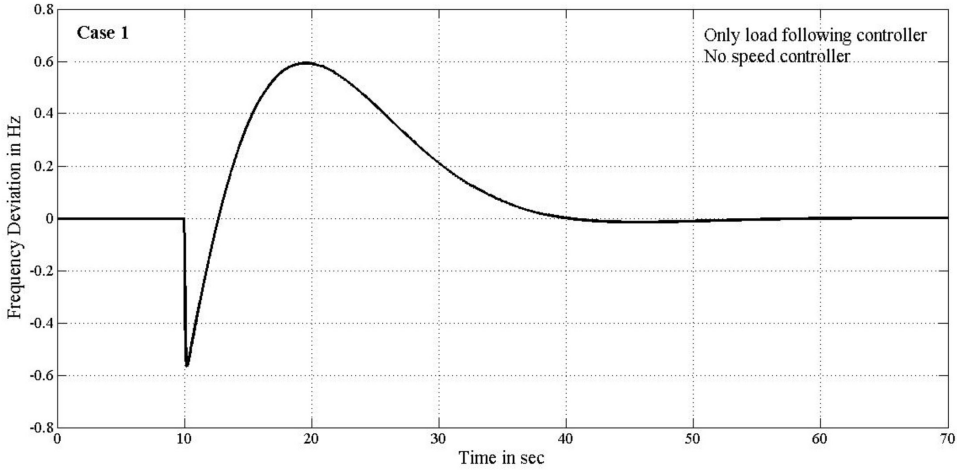

Figure 3: Frequency deviation of MTG system in Hz (Case-1)

Case 2:

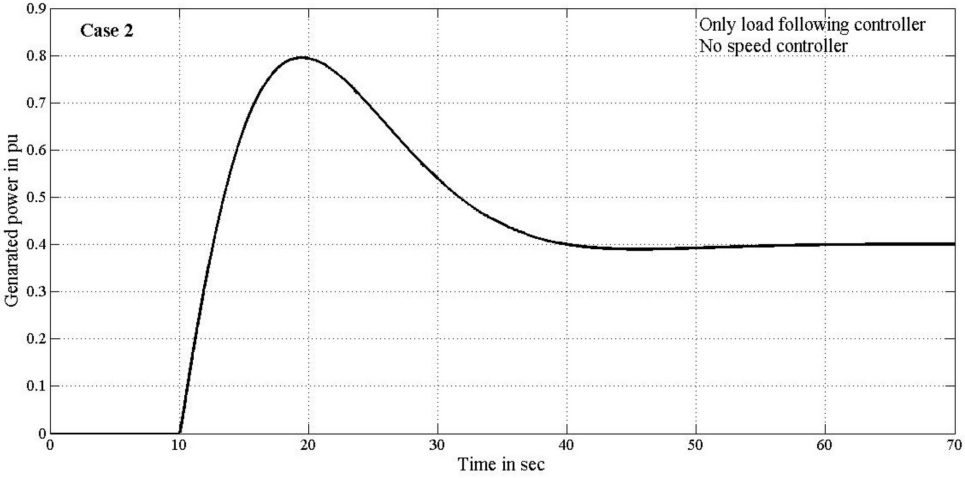

Figure 4: Generated power by MTG system in pu (Case-2)

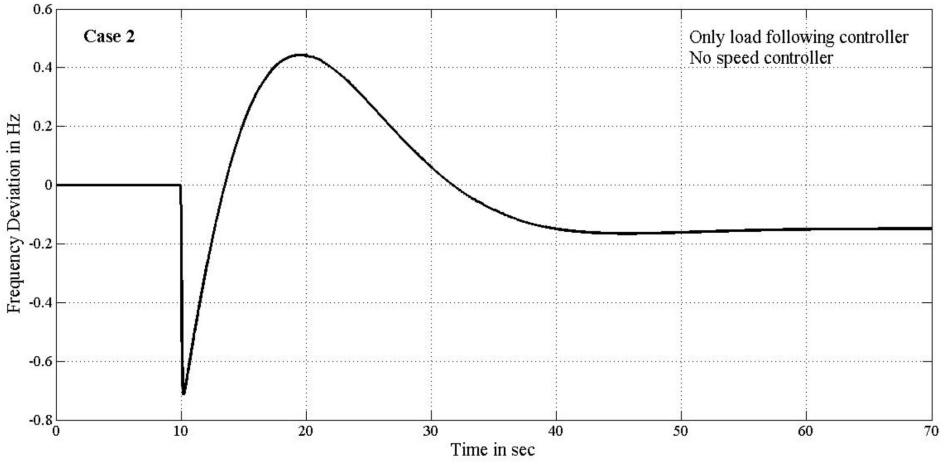

Figure 5: Frequency deviation of MTG system in Hz (Case-2)

Case 3:

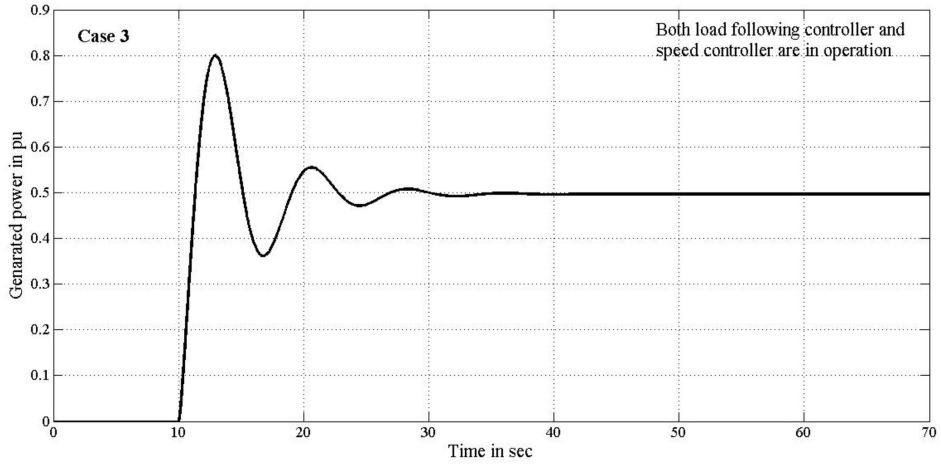

Figure 6: Generated power by MTG system in pu (Case-3)

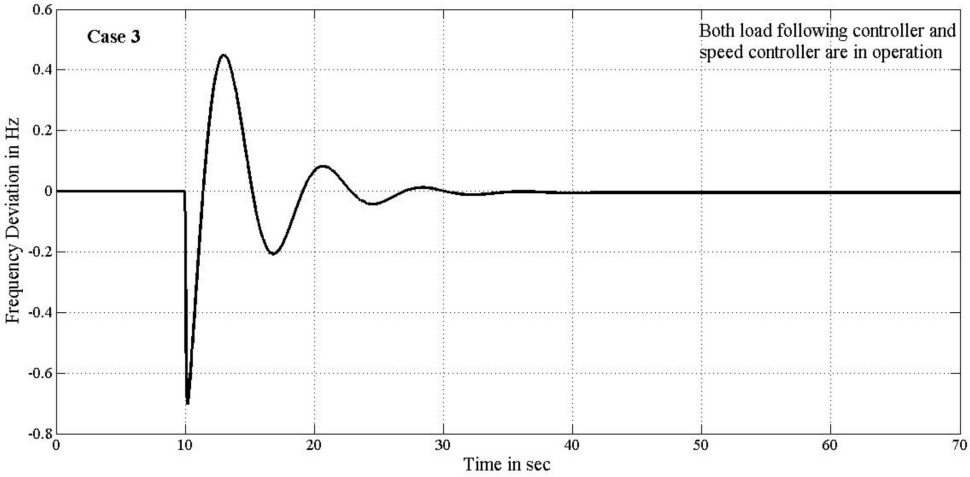

Figure 7: Frequency deviation of MTG system in Hz (Case-3)

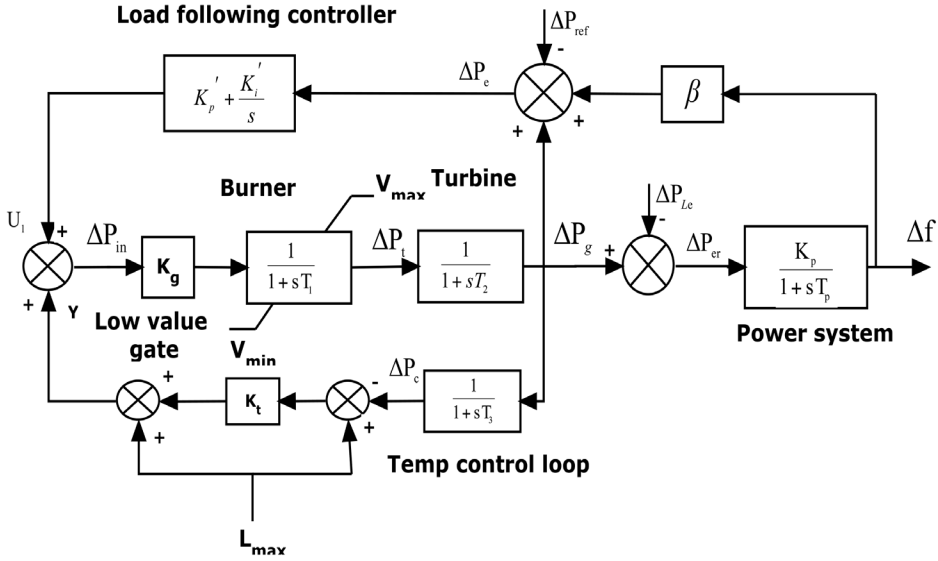

Figure 8: Block diagram representation of split-shaft MTG system when only load following controller is used with frequency deviation through a proportional gain (□) as an input signal to it.

Case-4:

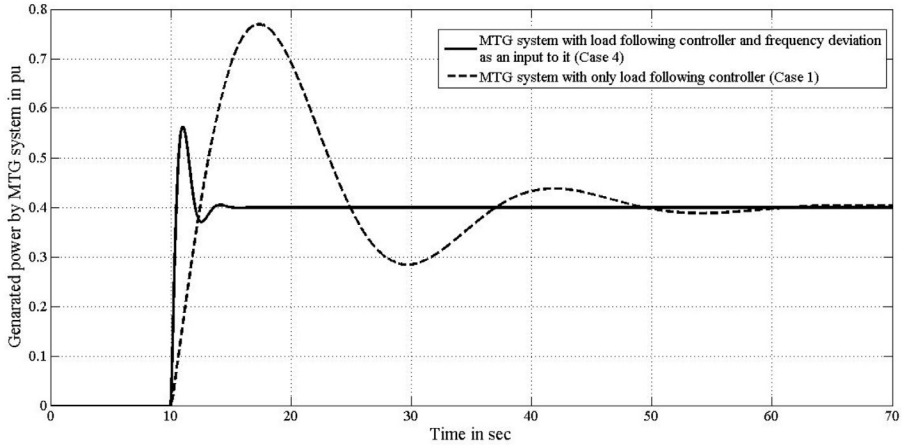

Figure 9: Comparison of generated power by MTG system in pu between Case-4 & Case-1

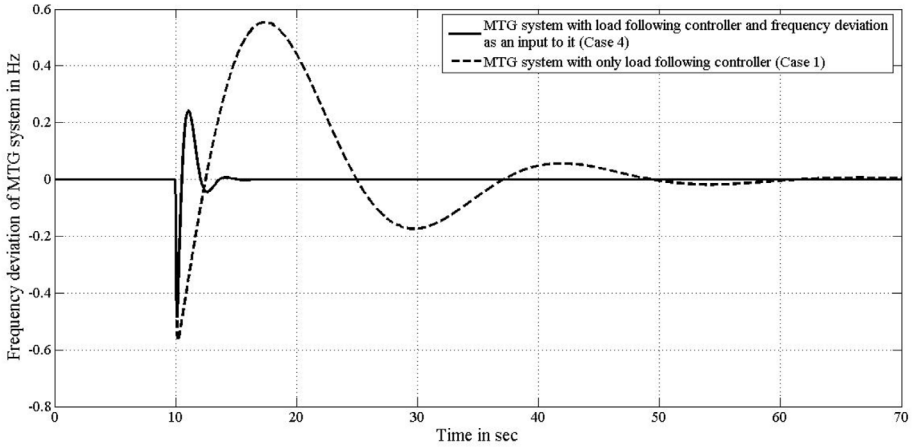

Figure 10: Comparison of frequency deviation of MTG system in Hz between Case-4 & Case-1

Case-5:

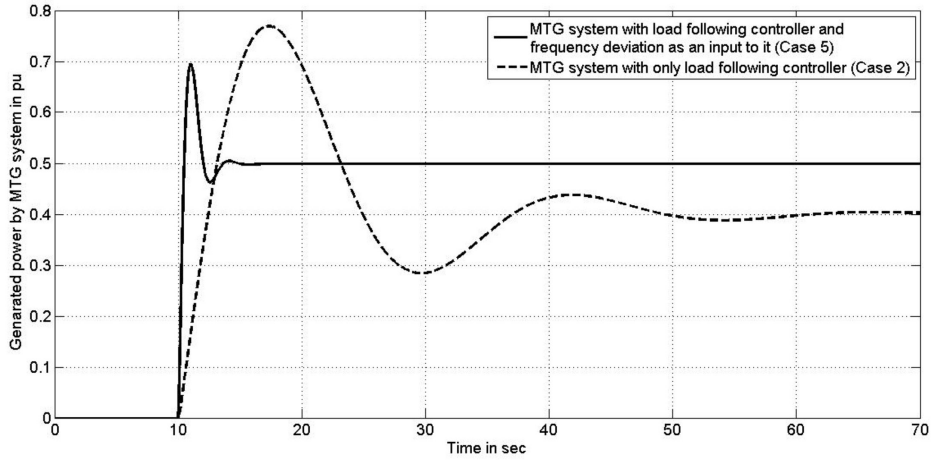

Figure 11: Comparison of generated power by MTG system in pu between Case-5 & Case-2

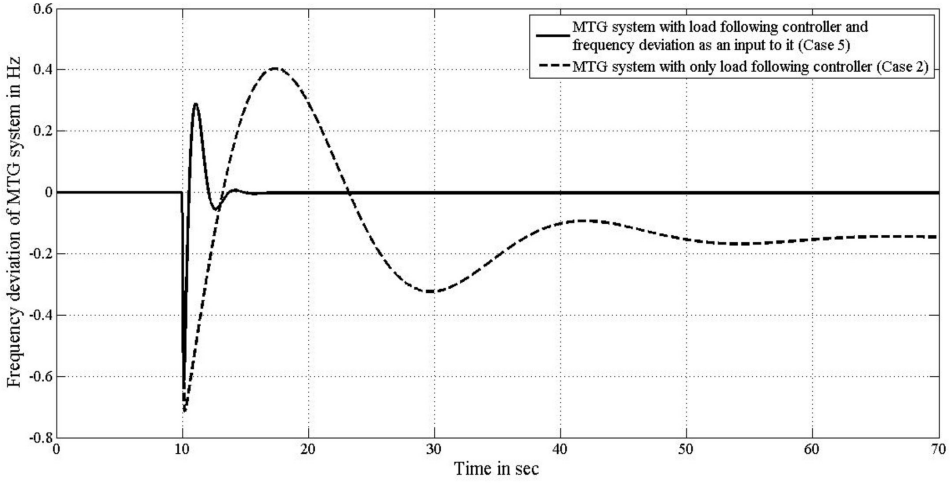

Figure 12: Comparison of frequency deviation of MTG system in Hz between Case-5 & Case-2

Case 6:

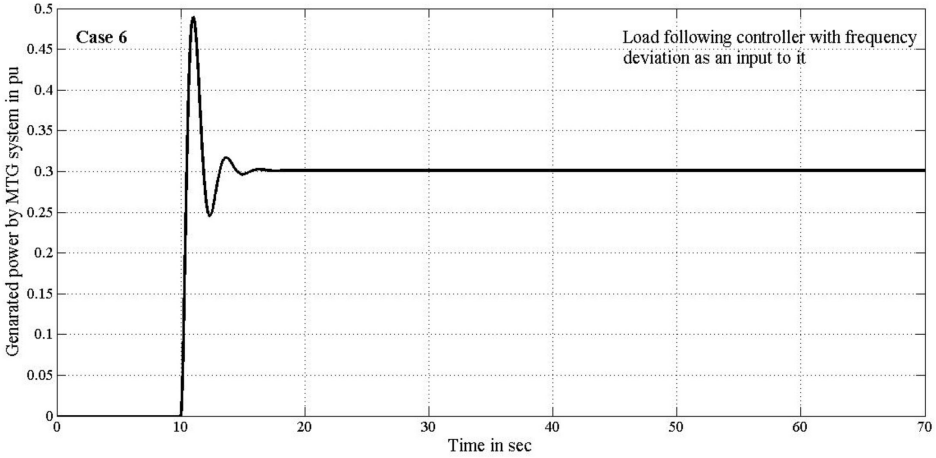

Figure 13: Generated power by MTG system in pu (Case-6)

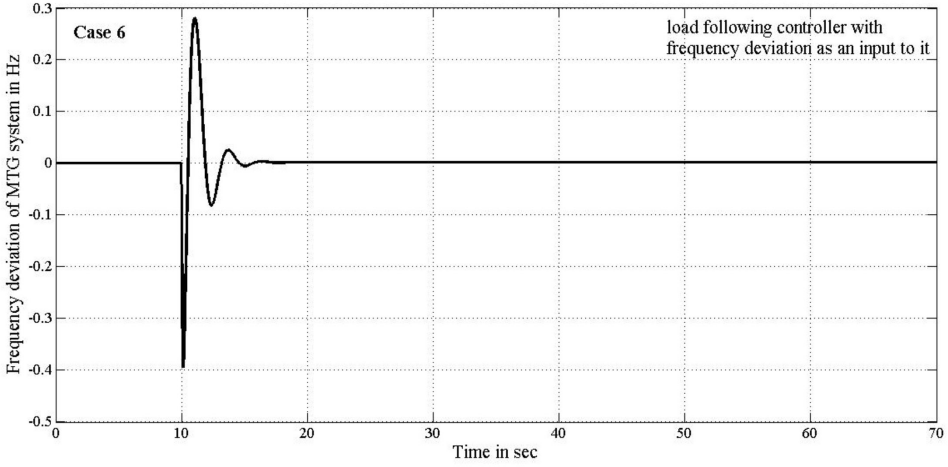

Figure 14: Frequency deviation of MTG system in Hz (Case-6)

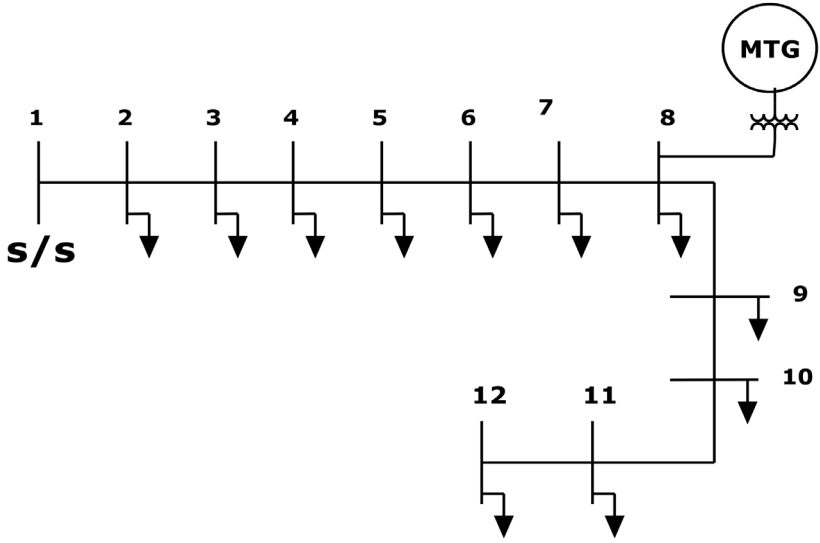

Figure 15: 12 node radial distribution network with MTG system connected at node 8.

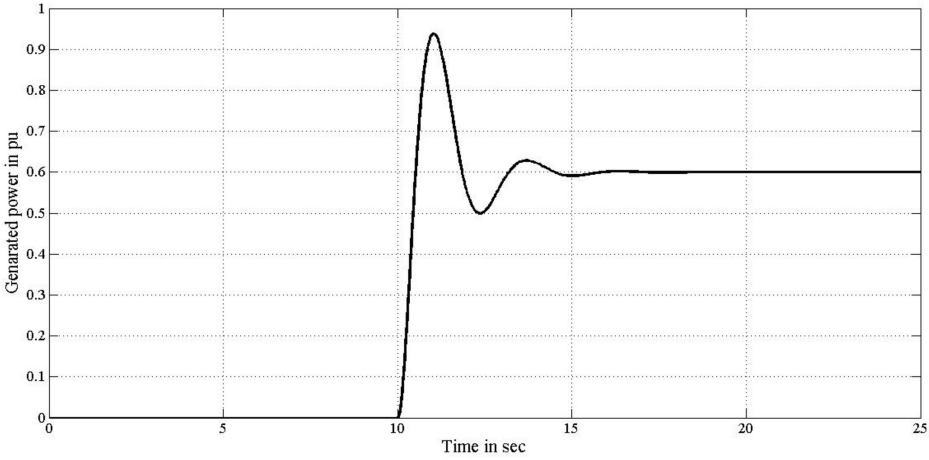

Figure 16: Active power generation By MTG system in pu when connected to a 12 node distribution network.

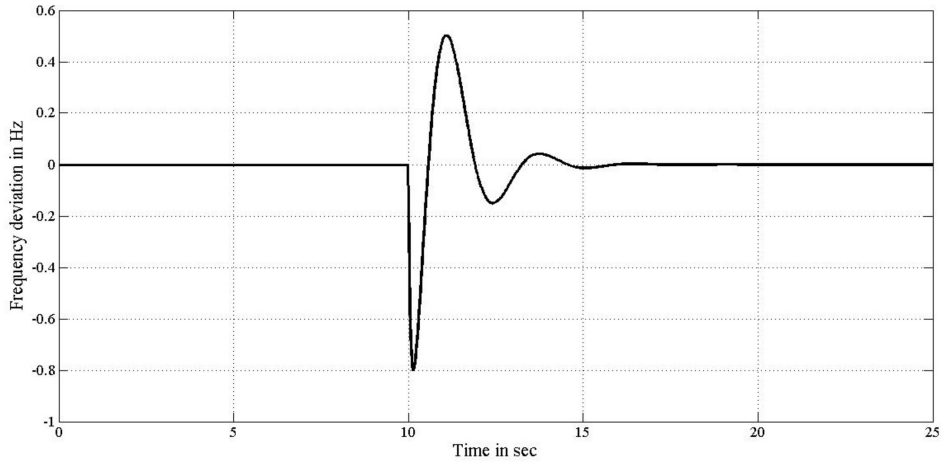

Figure 17: Frequency deviation of MTG system in Hz when connected to a 12 node distribution network.

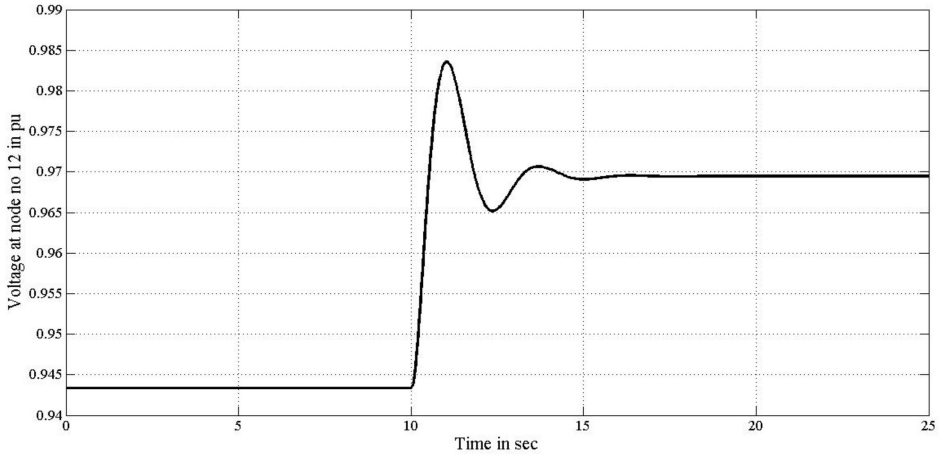

Figure 18: Voltage magnitude of node no 12 in pu when MTG connected to a 12 node distribution network.

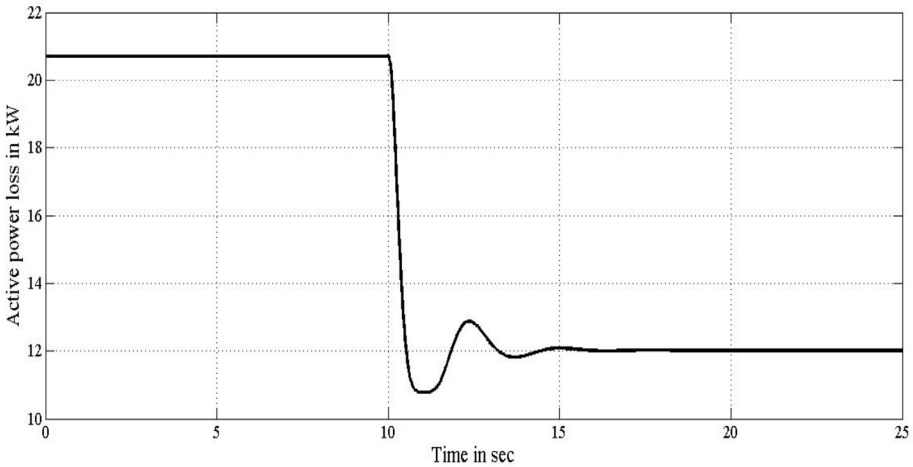

Figure 19: Active power loss of the 12 node distribution network in kW when MTG connected to a 12 node distribution network.

TABLE 1: Voltage magnitudes of 12 nodes of distribution network Node no Voltage magnitudes (pu) without MTG system Voltage magnitudes (pu) with MTG system connected at node 8

Node no	Voltage magnitudes (pu) without MTG system	Voltage magnitudes (pu) with MTG system connected at node 8
1	1.0000	1.0000
2	0.9943	0.9958
3	0.9890	0.9920
4	0.9806	0.9864
5	0.9698	0.9799
6	0.9665	0.9780
7	0.9637	0.9766
8	0.9553	0.9739
9	0.9473	0.9733
10	0.9445	0.9705
11	0.9436	0.9697
12	0.9434	0.9695

TABLE 2: Parameters of split-shaft MTG system model

Parameters	Representation	Value
P_r	Rated Real power generation capacity	250 kW
T_1	Fuel system lag time constant 1	10.0 s
T_2	Fuel system lag time constant 2	0.1 s
T_3	Temperature control loop lag time constant	3.0 s
K_g	Low value gate	0.7
K_t	Temperature control loop gain	1.0
D	Damping of generator	0.667
H	Inertia of generator	0.86
V_{max}	Maximum value position	1.2
V_{min}	Minimum value position	-0.1
L_{max}	Temperature control loop reference	1.2
$K_p^{'}$	Proportional gain of load following controller	-3.5
$K_i^{'}$	Integral gain of load following controller	-6.0
$K_p^{''}$	Proportional gain of speed controller	-0.4
$K_i^{''}$	Integral gain of speed controller	-0.85
β	Proportional frequency gain	50.0

TABLE 3: Parameters of 12 node distribution network

Branch no.	Sending end node no.	Receiving end node no.	Branch resistance (ohm)	Branch reactance (ohm)	Active power load at receiving end node (kW)	Reactive power load at receiving end node (kVAr)
1	1	2	1.093	0.455	60	60
2	2	3	1.184	0.494	40	30
3	3	4	2.095	0.873	55	55
4	4	5	3.188	1.329	30	30
5	5	6	1.093	0.455	20	15
6	6	7	1.002	0.417	55	55
7	7	8	4.403	1.215	45	45
8	8	9	5.642	1.592	40	40
9	9	10	2.890	0.818	35	30
10	10	11	1.514	0.428	40	30
11	11	12	1.238	0.351	15	15

ABOUT THE AUTHORS

Bikash Das is doing his M.Tech Degree at Indian Institute of Technology, Kharagpur. e-mail: bcazdas@gmail.com

Debapriya Das received his B.E. degree from Calcutta University, Calcutta, India, M.Tech. degree from Indian Institute of Technology, Kharagpur, and Ph.D. degree from Indian Institute of Technology, New Delhi, India. Currently, he holds the position of Professor at Indian Institute of Technology, Kharagpur, India. He is also faculty advisor of power and energy system group. He is also the coordinator of three years M.Tech. Program in Electrical Engineering. His research interests are operation of electric power distribution, microgrid and power system operation control. e-mail: ddas@ee.iitkgp.ernet.in